

Evolution of rotated Brass texture by cross rolling: implications on formability

Sumeet Mishra, Mirtunjay Kumar & Amit Singh

To cite this article: Sumeet Mishra, Mirtunjay Kumar & Amit Singh (2020) Evolution of rotated Brass texture by cross rolling: implications on formability, Materials Science and Technology, 36:12, 1272-1281, DOI: [10.1080/02670836.2020.1773036](https://doi.org/10.1080/02670836.2020.1773036)

To link to this article: <https://doi.org/10.1080/02670836.2020.1773036>



View supplementary material [↗](#)



Published online: 04 Jun 2020.



Submit your article to this journal [↗](#)



Article views: 147




View related articles [↗](#)



View Crossmark data [↗](#)

Evolution of rotated Brass texture by cross rolling: implications on formability

Sumeet Mishra, Mirtunjay Kumar  and Amit Singh

Department of Materials Science and Engineering, Indian Institute of Technology Kanpur, Kanpur, India

ABSTRACT

In the present work, the possibilities of tailoring crystallographic texture via cross rolling are presented. It is shown that a strong rotated Brass texture develops upon cross rolling in aluminium alloys which also remains intact during the subsequent recrystallisation annealing treatment. The governing mechanisms behind the evolution of deformation and recrystallisation texture are discussed in terms of effect of strain path on stability of deformation texture components and strain-induced boundary migration mechanism, respectively. In addition, the likelihood of rotated Brass texture having a positive effect on formability is discussed in terms of sluggish cross-slip criteria as the rotated Brass texture presents a unique scenario where cross-slip is inhibited along all the three principal directions.

ARTICLE HISTORY

Received 1 April 2020
Revised 17 May 2020
Accepted 19 May 2020

KEYWORDS

Cross rolling; texture; cross-slip; formability; Al alloys

Introduction

Sheet metal forming is a widely used manufacturing process owing to several advantages such as good quality finished products, dimensional accuracy and suitability for large batches which in turn gradually reduces the initial tooling costs [1–3]. It can be employed to make wide range of products from soft drink cans to automotive car bodies [1–3]. Therefore, a considerable amount of research has been carried out over the years to improve the understanding of sheet metal forming process especially with respect to localised necking which can grow rapidly to cause tearing and failure [4]. It is now well accepted that in situations where the major strain is positive and minor strain is negative (second quadrant of forming limit curve), localised necking will occur when the tension reaches a maximum [4]. The maximum tension criterion is shown schematically in Figure 1(a). It can be observed that maximum tension criterion provides a reasonable estimate of the localised necking strains for conditions ranging from uniaxial (point B) to plain strain (point A) and can be expressed as [4].

$$\varepsilon_1 + \varepsilon_2 = n \quad (1)$$

Here, ε_1 and ε_2 are the major and minor strains, respectively and n is the strain hardening exponent. It should be noted that the maximum tension criterion is valid between uniaxial and plain strain conditions as there exists a direction of zero extension for all these tests [4]. However, there is no direction in which extension

is zero when both major and minor strains are positive, namely in the first quadrant (biaxial conditions) [4]. Therefore, the maximum tension criterion is no longer valid as can be seen from Figure 1(a) where the forming limit curve does not follow the maximum tension line. Nevertheless, it is evident from Figure 1(a) that plain strain condition (marked as 'A') corresponds to the lowest point on the forming limit curve and hence the overall formability of sheets can be improved by raising the point A upwards (Figure 1(b)). Considering Equation (1), point A corresponds to

$$\varepsilon_1 = n \quad (2)$$

Hence, increasing the strain hardening exponent (n) will delay the onset of localised necking and improve the formability of sheets. For other conditions, such as uniaxial loading, increasing ' n ' will also have a beneficial effect on formability as can be envisioned from Equation (1). There have been several studies in literature also where the positive effect of strain hardening on formability is confirmed [5,6]. However, strain hardening exponent ' n ' is an empirical parameter and does not reveal any correlation between microstructural features and strain hardening. Therefore, it is difficult to devise strategies based on ' n ' to improve the strain hardening ability of the material.

In this regard, the Kocks-Mecking model [7,8] where strain hardening behaviour is interpreted as the competition between athermal storage of dislocations and thermally activated annihilation of dislocations is of

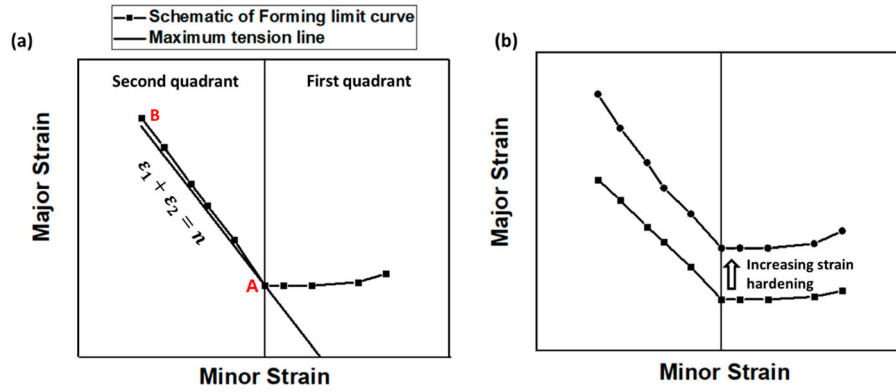


Figure 1. (a) Schematic of forming limit curve and maximum tension criterion and (b) schematic of forming limit curve illustrating the beneficial effect of strain hardening on formability.

considerable importance as microstructurally sensitive parameters can be incorporated in this model which in turn can provide crucial insights to improve the strain hardening ability of the material. The prototype Kocks-Mecking model can be expressed as

$$\frac{d\rho_f}{d\varepsilon_p} = M \left(\frac{d\rho_{\text{storage}}}{d\varepsilon_p} - \frac{d\rho_{\text{annihilation}}}{d\varepsilon_p} \right) \quad (3)$$

Here, the left-hand side of the equation ($d\rho_f/d\varepsilon_p$) represents the evolution of forest dislocations (ρ_f) during plastic deformation which depends on the competition between storage and annihilation and M is Taylor factor which depends upon the texture of the material. The rate of storage of dislocations is inversely related to the dislocation mean free path in the glide plane, namely average obstacle spacing (L), whereas the rate of annihilation is directly proportional to forest dislocation density [7,8]. Hence, Equation (3) can be re-written as

$$\frac{d\rho_f}{d\varepsilon_p} = M \left(\frac{1}{bL} - K_2\rho_f \right) \quad (4)$$

Since the mean free path (L) is inversely proportional to $\rho_f^{1/2}$, irrespective of arrangement of dislocations, Equation (4) can be modified as

$$\frac{d\rho_f}{d\varepsilon_p} = M(K_1\rho_f^{1/2} - K_2\rho_f) \quad (5)$$

Here, K_1 and K_2 are constants related to dislocation accumulation and annihilation, respectively [7,8]. It should be noted that dislocation annihilation takes place mainly via cross-slip and therefore ' K_2 ' represents the cross-slip probability [9]. The ease of cross-slip is strongly orientation dependent and as shown later in the paper plays a key role in deciding the onset of necking.

In order to obtain the plastic response of the material, Equation (5) is used in combination with Taylor equation (Equation (6)) to derive the well-established

Voce hardening equation (Equation (7)).

$$\sigma = \sigma_y + \alpha M G b \rho_f^{1/2} \quad (6)$$

$$\sigma = \sigma_y + \frac{M \alpha G b K_1}{K_2} \left(1 - \exp \left(-\frac{M K_2}{2} \varepsilon_p \right) \right) \quad (7)$$

Here, σ_y is the yield strength, G is the shear modulus, b is Burgers vector and α is a constant (~ 0.3). As can be observed from Equation (7), the material response, especially the strain hardening behaviour can now be understood in terms of physical parameters ' K_1 ' and ' K_2 '.

Taking forward the Voce hardening equation, it can be combined with Considere's criteria to derive the expression for necking strain (ε_N) in an approach similar to that of Yasnikov et al. [10] and Vinogradov et al. [11].

$$\varepsilon_N = \frac{2}{M K_2} \ln \left[\frac{1 + \frac{M K_2}{2} \frac{\sigma_y}{\sigma}}{1 + \frac{M \alpha G b K_1}{K_2}} \right] \quad (8)$$

As can be observed from Equation (8), all the parameters specified in the Kocks-Mecking model (Equation (5)) and Taylor equation (Equation (6)) enter into the expression for the onset of necking. However, contribution from the factors specified within the logarithmic bracket would be significantly less compared to the pre-logarithmic factors, namely Taylor factor ' M ' and cross-slip probability ' K_2 '. As mentioned previously, both these parameters are not independent of each other as they are orientation dependent.

In order to determine the sensitivity of necking strain (ε_N) towards Taylor factor ' M ' and cross-slip probability ' K_2 ', we illustrate the true stress versus true strain curves of Al single crystals oriented along [001] and [111] in Figure 2. The experimental data was taken from the works of Hosford et al. [12]. These orientations were chosen as they represent the lower and upper limit of both Taylor factor and cross-slip probability. The Taylor factor varies from 2.44 for [001] orientation (lower limit) to 3.67 for [111] orientation (upper

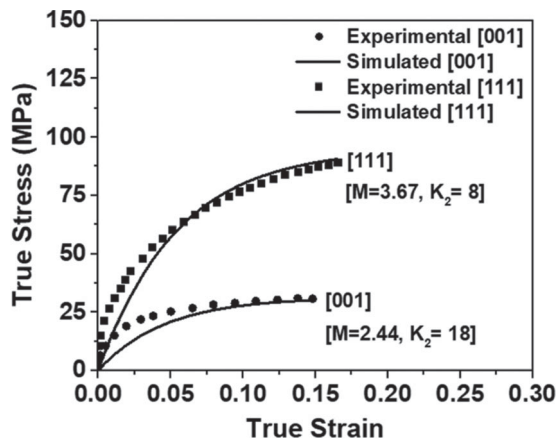


Figure 2. Experimental and simulated stress-strain curves of [001] and [111] Al single crystals at room temperature. The experimental data was taken from the works of Hosford et al. and the simulated curves correspond to Equation (7).

limit). On the other hand, ' K_2 ' varies from 8 for [111] orientation (lower limit) to 18 for [001] orientation (upper limit). The value of K_2 was determined by fitting the experimental curves with Voce hardening equation. The methodology for calculation of Taylor factor is explained in detail elsewhere [13,14]. As the orientation of tensile axis changes from [001] to [111], there is an increase in Taylor factor by 1.5 times, whereas the cross-slip probability decreases by 2.25 times. Considering Equation (8), it can be envisioned that the negative effect of increase in Taylor factor would be compensated by decrease in cross-slip probability which in turn will increase the necking strain. Therefore, the possible strategies for increasing necking strain should focus more on K_2 compared to M as the cross-slip probability can change by several times by tuning the texture and microstructural features (~ 3 – 5 times), whereas Taylor factor can only change by a maximum of 1.5 times, namely from 2.44 to 3.67. As the theme of the present paper is to highlight the reduction in cross-slip probability by effective texture control, we will not elaborate on other microstructural features which are also known to affect dynamic recovery. There are several excellent studies in the literature where the effect of microstructural features such as solutes and precipitates on cross-slip probability are discussed [15,16].

As shown in the previous paragraph, cross-slip probability is the least for orientations which have $\langle 111 \rangle$ direction \parallel loading axis (LA). On the other hand, cross-slip probability is the highest for orientations which have $\langle 001 \rangle$ direction \parallel LA. Therefore, effective texture control requires formulating ways to develop $\langle 111 \rangle \parallel$ LA texture. The sluggish cross-slip in $\langle 111 \rangle \parallel$ LA orientations has been discussed in great detail in the past and several explanations have been provided. Mori and Fujita [17] explained this behaviour in terms of Schmid factor for cross-slip system. As can be seen from Figure 3(a), the Schmid factor

for cross-slip system decreases with departure from the [001] axis and becomes zero on the line joining $\bar{1}12$ and [011] poles. This might be thought of as a reason for decreasing cross-slip with deviation away from [001] axis. As the loading axis approaches the $\bar{1}11$ axis, the value of Schmid factor increases, albeit the sign is negative. This suggests that for $\bar{1}11 \parallel$ LA grains, the resolved shear stress on cross-slip plane has a direction opposite to that favouring the cross-slip process, whereas for [001] \parallel LA grains, resolved shear stress favours the cross-slip process. This can be understood clearly from Figure 3(b) where the ratio of Schmid factor for cross and primary slip system is shown. The ratio varies from 1 for [001] orientation to -1 for $\bar{1}11$ orientation. Kubin et al. [18,19] have defined these scenarios as acute and obtuse cross-slip, respectively. It is generally agreed that acute annihilation is more difficult compared to obtuse annihilation. Another possible explanation is provided in terms of ratio of Schmid factor for the leading and trailing partial dislocation [17]. It can be observed from Figure 3(c) that the ratio is around 2 for $\bar{1}11 \parallel$ LA grains compared to 0.5 for [001] \parallel LA grains. This suggests that primary dislocations are widely extended under the action of external stress for $\bar{1}11$ orientation whereas the extended dislocations tend to shrink for [001] \parallel LA grains.

As is clear from the above paragraph, texture control in terms of $\langle 111 \rangle \parallel$ LA is essential to deter cross-slip and hence improve the strain hardening ability and the necking strain. As is well known, out of different types of automotive materials, steels have the best formability owing to the favourable $\langle 111 \rangle \parallel$ ND (normal direction), namely gamma fibre texture. This favourable texture in steels can simply be obtained by rolling followed by recrystallisation annealing treatment [20]. On the other hand, Al alloys which have an advantageous strength to weight ratio compared to steels and can satisfy the global call for reduction in carbon emission lag behind because of poor formability. This poor formability is mainly due to a strong cube texture ($\langle 001 \rangle \parallel$ LA) developed in Al alloys after rolling and recrystallisation/solution annealing treatment (O or W temper) [21]. It should be noted that most forming operations are done in this soft temper conditions. Therefore, texture control assumes a much more important role in Al alloys compared to steels. Therefore, in order to carry out the present work, we have selected an age hardenable aluminium–magnesium–silicon alloy which is a standard workhorse alloy in automotive industries. These AA 6xxx series alloys are routinely used for making car bodies and any improvement in formability of these alloys will be of tremendous importance to the automotive industries. In the following sections, we will describe the experimental methodology for obtaining $\langle 111 \rangle \parallel$ LA texture followed by discussions regarding the mechanisms behind the evolution of this advantageous texture.

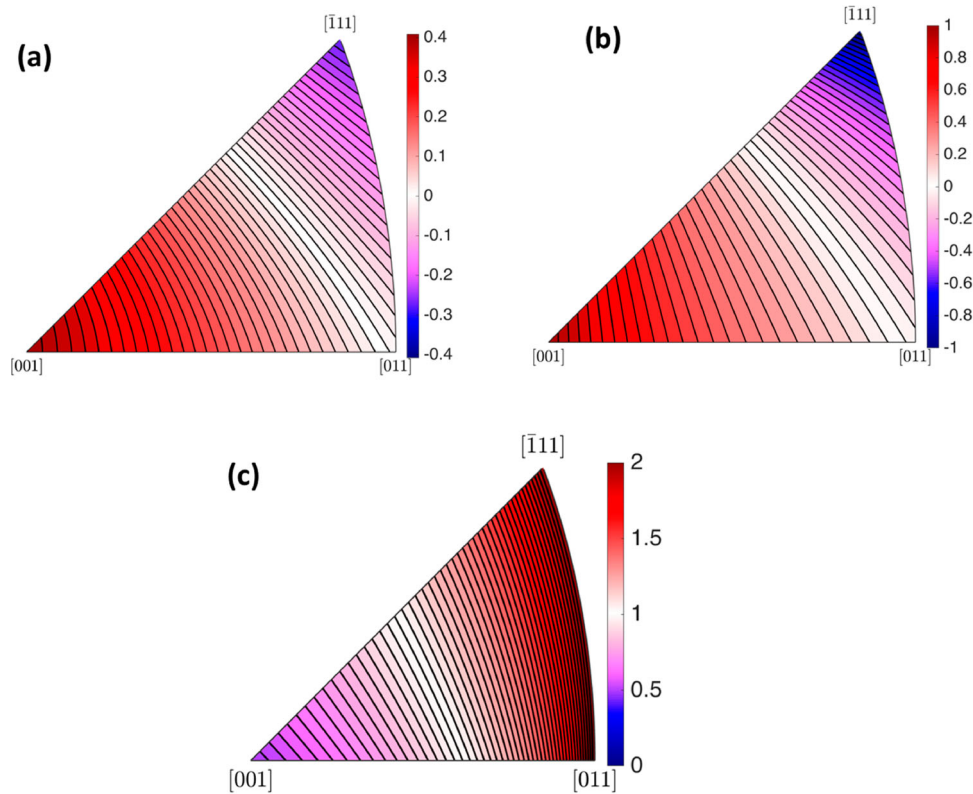


Figure 3. (a) Schmid factor for cross-slip system $(\bar{1}\bar{1}1)[\bar{1}01]$, (b) ratio of Schmid factor for cross and primary slip system $((111)[\bar{1}01])$ and (c) ratio of Schmid factor for leading $(\frac{1}{6}[\bar{2}11])$ and trailing $(\frac{1}{6}[\bar{1}\bar{1}2])$ partial.

Experimental details

As is well known, rolling is the most important and widely used industrial process which plays a deciding role in determining the engineering properties and the ultimate formability of the material [22]. Therefore, tailoring the rolling process is one of the possible options for obtaining the favourable $\langle 111 \rangle \parallel$ LA texture. In this regard, changing the strain path during rolling has received considerable attention over the past several years. The most popular method of them is cross rolling where the rolling direction is turned through 90° after each pass [23,24]. This results in a tetragonal sample symmetry with a 4-fold axis along the ND (normal direction) compared to 2-fold axis of straight rolling. There have been several reports where it has been shown that cross rolling leads to a significantly different deformation and recrystallisation texture compared to straight rolling [23,24]. Therefore, in the present work, we have subjected the Al-Mg-Si alloy of composition (wt-%) 97.6Al–0.7Si–1Mg–0.3Cu–0.2Fe–0.17Cr–0.04Mn to 90% reduction in thickness by straight and cross rolling, respectively. The rolling process was carried out in increments of 23 passes with each pass corresponding to a true strain of -0.1 . It should be noted that the samples were subjected to solution annealing treatment at 550°C for two hours prior to rolling so as to remove the previous thermo-mechanical history. The rolled samples were then annealed at 300°C for two

hours to complete the recrystallisation process. The recrystallisation time was decided based on hardness measurements which are shown later in the paper.

Following the thermo-mechanical treatments, texture measurement of the rolled and recrystallised samples was undertaken by measuring three incomplete pole figures (111), (200) and (220) at the mid plane of the samples. The pole figures were measured upto a tilt angle of 70° to avoid defocusing error at higher tilt angles. For each tilt, the sample was rotated from 0 to 360° during measurements. A Rigaku four circle goniometer was used for these texture measurements. The plotting of ODF (orientation distribution function) sections was performed using ResMat software. The microstructural observations of the recrystallised samples were carried out via electron back scatter diffraction (EBSD). A JEOL field emission gun microscope equipped with Oxford Nordlys detector was used for this purpose. A step size of $1\ \mu\text{m}$ was used for EBSD measurements. The hardness measurements were carried out with a Vicker's microhardness tester with a $500\ \text{g}$ load and dwell time of $10\ \text{s}$.

Results and discussion

The texture after the initial solution annealing treatment is provided in the supplementary file. It can be observed that the initial sample has a strong cube texture $\{001\} \langle 100 \rangle$ with intensity $42 \times$ random. This is

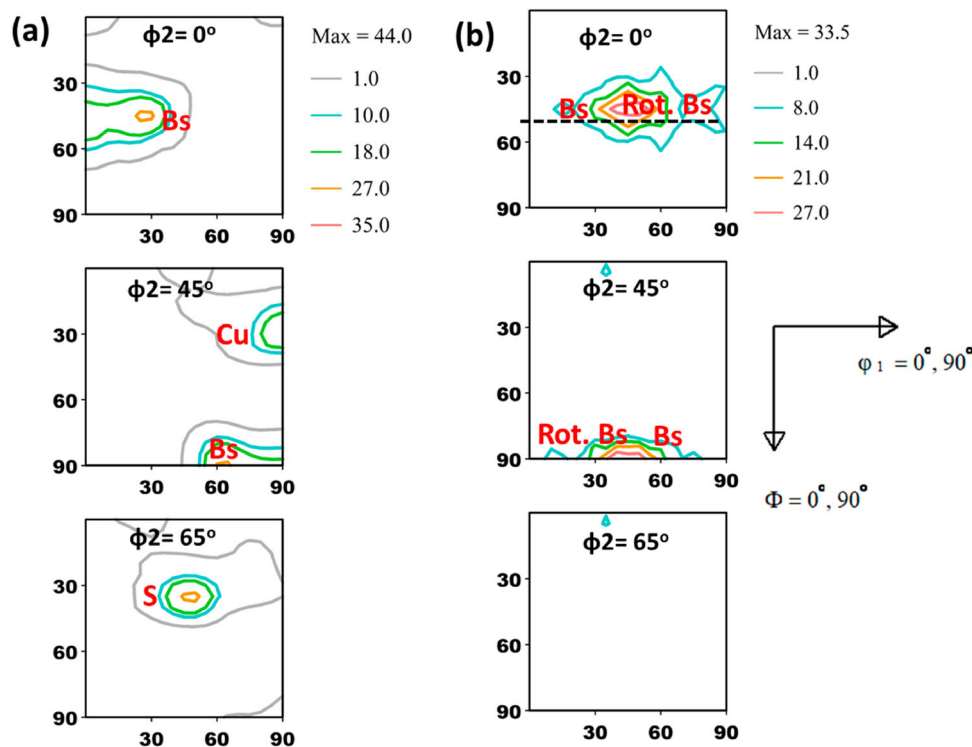


Figure 4. ODF sections after 90% rolling reduction (a) straight rolling and (b) cross rolling.

the usual texture observed in Al alloys after conventional processing and annealing treatment and is one of the foremost reasons for poor formability due to extensive cross-slip [17].

Texture evolution after 90% rolling for the straight and cross rolled samples is shown via important ODF sections ($\varphi_2 = 0^\circ, 45^\circ$ and 65°) in Figure 4(a,b). The texture for the straight rolled sample can be characterised by the presence of Copper $\{112\}\langle 11\bar{1}\rangle$, S $\{123\}\langle 63\bar{4}\rangle$ and Brass $\{110\}\langle 1\bar{1}2\rangle$ components. These texture components are marked as Cu, S and Bs in the ODF sections in Figure 4(a). This is the typical rolling texture observed in medium and high stacking fault energy materials and is commonly known as ‘Copper type texture’ or ‘Pure metal type texture’ [25,26]. On the other hand, the rolling texture for cross rolled sample is distinctly different. The texture can be characterised by the presence of strong rotated Brass $\{110\}\langle 1\bar{1}1\rangle$ component with some spread along the alpha fibre towards the Brass position. The alpha fibre is marked as a black dashed line in Figure 4(b). The most distinctive feature is the absence of Copper and S component in the cross rolled sample compared to straight rolled sample.

Following the rolling process, the samples were recrystallised at 300°C for two hours. As can be seen from Figure 5(a), there is a sharp drop in hardness in the initial one hour of annealing followed by a plateau after two hours. Hence, two hours at 300°C was selected for the recrystallisation process. The image quality maps shown in Figure 5(b) also corroborate that recrystallisation is more or less complete. The ODF sections of the

recrystallised samples are shown in Figure 6(a,b). It can be observed that there are stark differences between the textures of both the samples. The straight rolled sample develops a pronounced $\{001\}\langle 100\rangle$ Cube texture with intensity of $50\times$ random. On the other hand, cross rolled sample develops a rotated Brass texture. There is no indication of the presence of Cube component in the cross rolled sample. It should be noted that Miller indices of the rotated Brass component is $\{110\}\langle 1\bar{1}1\rangle$, namely $[1\bar{1}1]$ direction parallel to rolling direction (RD) or the loading axis. This can be illustrated elegantly via inverse pole figures in Figure 7(a,b). For the straight rolled sample, all the inverse pole figures show $[001]$ orientation parallel to RD, TD and ND, respectively. However, the cross rolled sample shows $[111] \parallel$ to RD, $[112] \parallel$ TD and $[110] \parallel$ ND. As illustrated previously in Figure 3, for all these three orientations, cross-slip is sluggish compared to $[001]$ orientation. Hence, cross rolled sample has an advantageous texture w.r.t to loading along any of the three principal directions, whereas straight rolled sample has unfavourable $[001]$ along all the principal directions. Therefore, it can be established that cross rolling has a favourable effect on the evolution of recrystallisation texture.

It should be noted that the material is in soft condition after the recrystallisation anneal treatment. Considering the beneficial texture of the cross rolled sample, it is ideally suited for forming operations at room temperature following which it can be solution treated and paint baked ($180^\circ\text{C}/30\text{ min}$) to achieve higher strength levels via precipitation hardening. Taking into account the above-presented results, we suggest an alternate

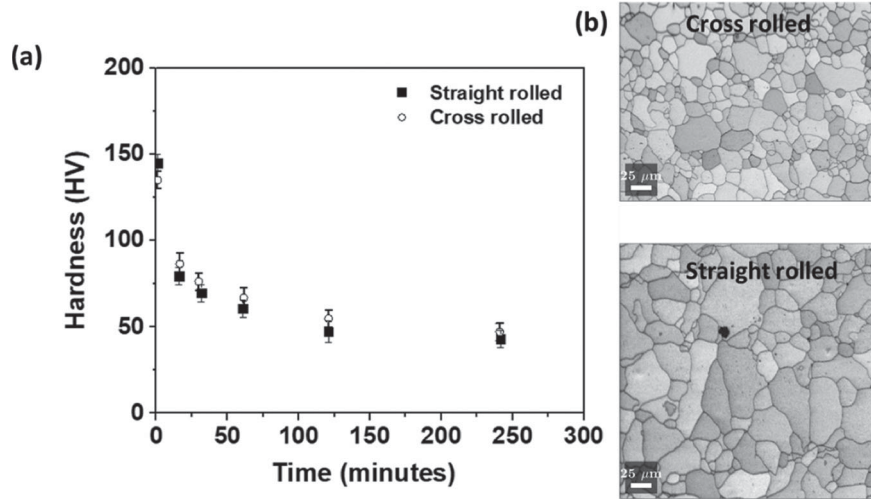


Figure 5. (a) Hardness evolution with time for straight and cross rolled samples and (b) image quality maps of straight and cross rolled samples after annealing at 300°C for two hours.

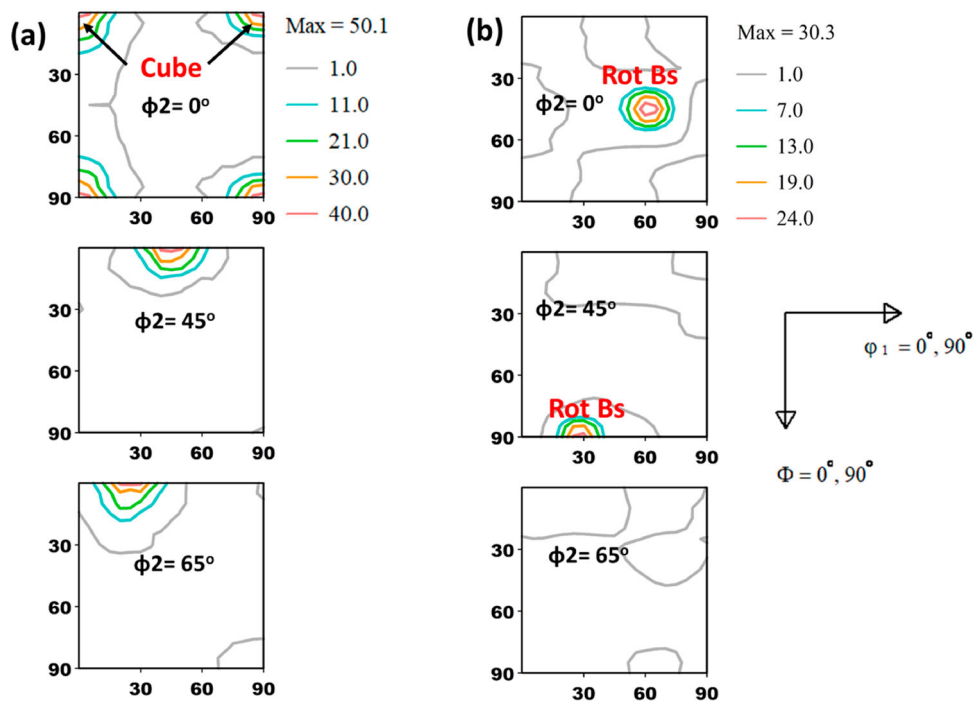


Figure 6. ODF sections after recrystallisation treatment (a) straight rolling and (b) cross rolling.

processing chain (Figure 8(b)) to improve the formability of Al alloys.

In order to understand the mechanism behind evolution of rotated brass texture during recrystallisation annealing treatment of cross rolled sample, we have to first analyse texture evolution during deformation as it is well known that deformation texture has a strong influence on recrystallisation texture. As shown in Figure 4(a), the straight rolled sample develops a Copper type texture which can be described by the presence of Copper, S and Brass components. The evolution of this Copper type texture from the initial Cube texture can be understood from the schematic shown in Figure 9(a). The initial Cube grains rotate towards the Goss position following which it moves along the alpha fibre towards Brass position and subsequently

along the beta fibre towards Copper orientation via S orientation. This is a well-established rotation path for Cube grains and has been discussed previously in many studies [27]. However, the lattice rotation rate depends upon the initial spread from ideal Cube position. The orientations which are within 5° of the ideal Cube position have a slower lattice rotation rate and can only reach the intermediate positions between Goss and Brass orientations. On the other hand, the orientations which have a larger deviation from the ideal Cube position ($> 5^\circ$, $\sim 10^\circ$) have a much faster lattice rotation rate and can traverse along the alpha and beta fibre to reach S and Copper position. Therefore, the experimental texture (Figure 4(a)) consists of a relative distribution of orientations along the alpha and beta fibre.

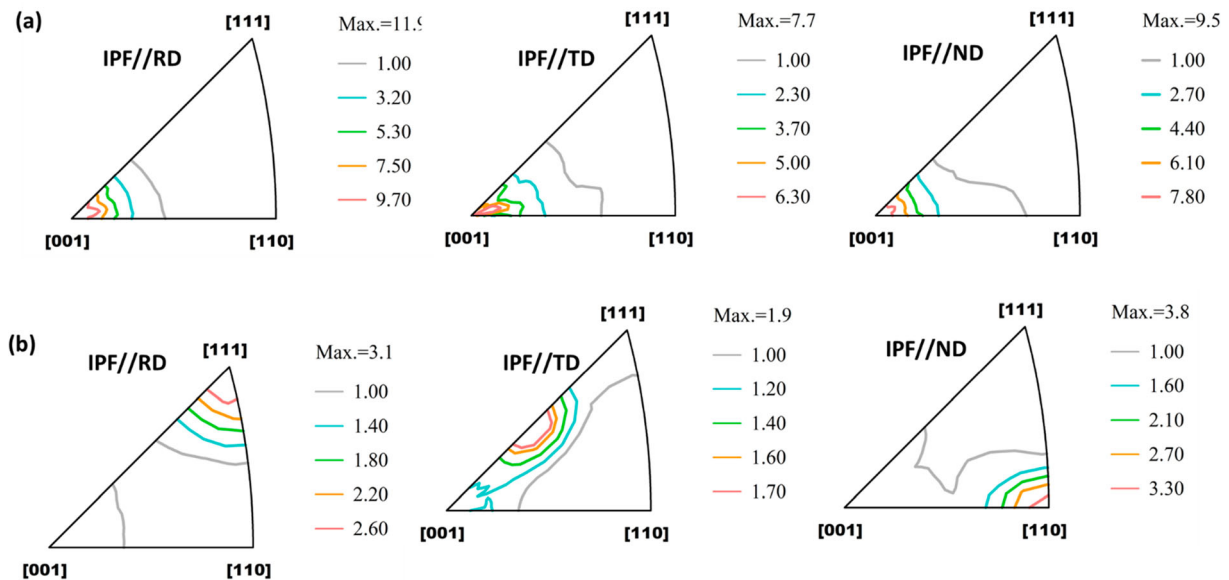


Figure 7. Inverse pole figures along rolling direction (RD), transverse direction (TD) and normal direction (ND) for (a) straight rolled and (b) cross rolled samples.

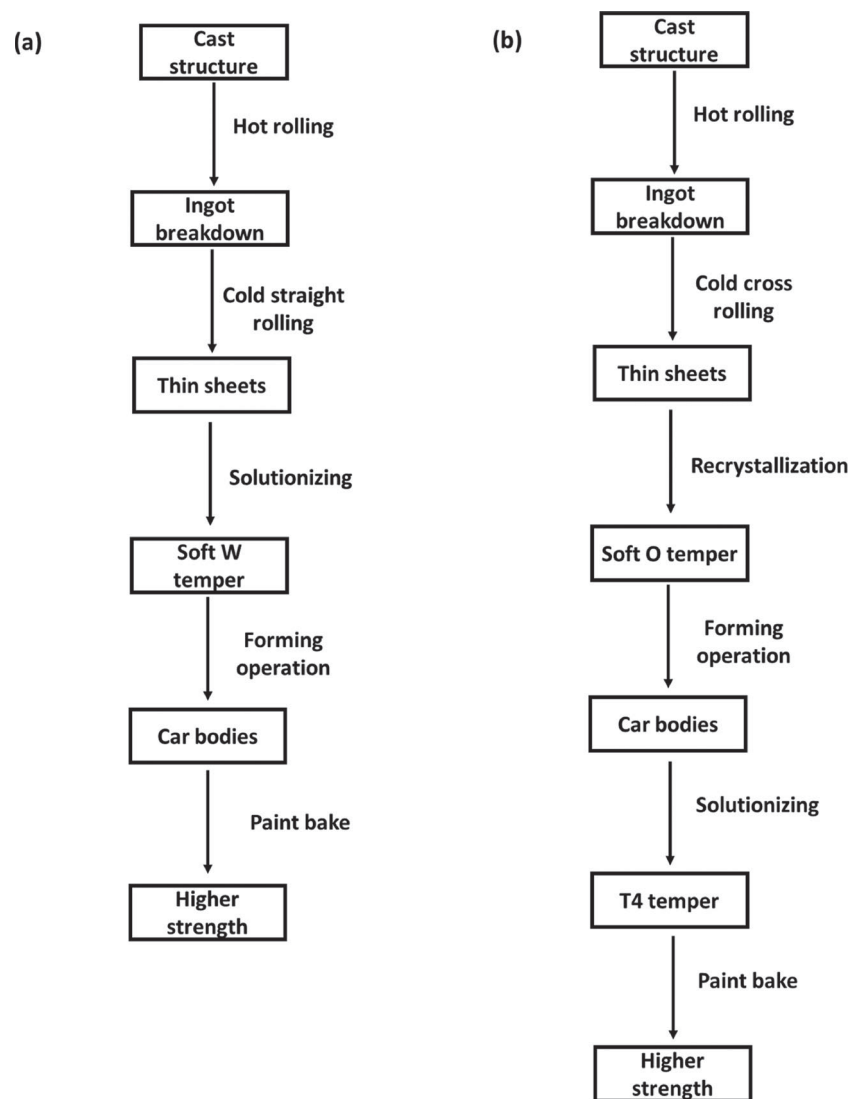


Figure 8. (a) Conventional processing chain and (b) alternate processing chain.

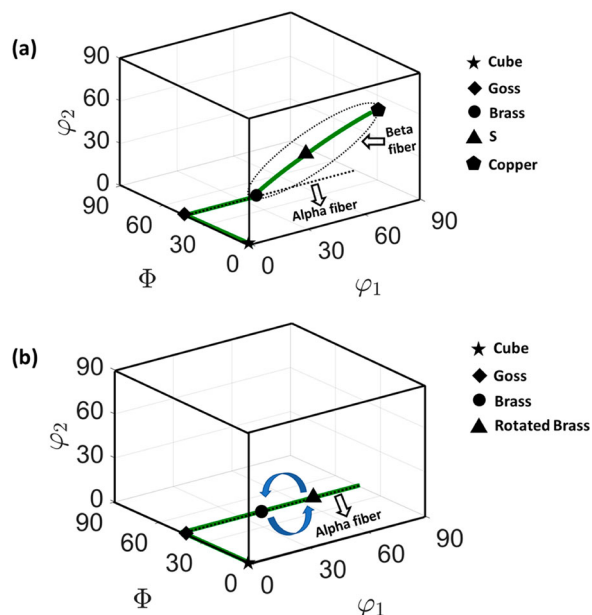


Figure 9. (a) Schematic of 3D ODF showing rotation of Cube orientation towards Copper orientation via alpha and beta fibre during straight rolling and (b) schematic of 3D ODF showing rotation of Cube orientation towards Brass and rotated Brass orientation during cross rolling.

However, for the cross rolled sample the situation is different. After the initial rolling along RD1, the Cube grains will follow the same rotation path as illustrated previously and will move along the alpha fibre to reach Brass position. Upon change in rolling direction by 90° for the second pass, the Brass orientation will move towards the rotated Brass position (Figure 9(b)). It has been illustrated via crystal plasticity simulations that rotated Brass is a stable orientation in the new reference frame for which the lattice rotation rate is zero [28]. Hence, during the second step rolling along RD2, the orientations will remain converged at rotated Brass position. For the third step rolling along RD1 where the sample is again rotated by 90°, the rotated Brass orientation will move back to Brass position which is a relatively stable end orientation with minimal lattice rotation rate in the original reference frame. Therefore, it can be said that during cross rolling, the orientations will keep moving back and forth between Brass and rotated Brass position and will not have any chance to move towards the beta fibre and reach S and Copper position. The back and forth movement between Brass and rotated Brass position is shown schematically via arrows in Figure 9(b).

The development of recrystallisation texture in straight rolled samples can be understood using the oriented growth theory. Several researchers in the past have used this theory to explain the evolution of Cube texture upon recrystallisation [29]. It is said that Cube grains prevail over other orientations because of their favourable growth into rolling texture components, especially Copper and S. Cube grains have a favourable

$40^\circ < 111 \rangle$ orientation relationship with these rolling texture components, which in turn favour their brisk growth compared to other orientations. However, these rolling texture components (Copper and S) are not present in the cross rolled sample (Figure 4(b)). Therefore, the preferred growth of Cube grains and the resulting strong Cube texture can be ruled out for the cross rolled sample.

The development of recrystallisation texture in cross rolled sample can be interpreted by analysing the competition between possible recrystallisation mechanisms, namely due to Cube bands, shear bands, deformation zone around large particles and grain boundaries. As mentioned in the previous paragraph, the role of Cube bands can be ruled out due to the absence of Copper and S component in the cross rolled sample.

Nucleation at shear bands is probable as the local dislocation density is quite high within the shear bands [29,30]. This provides a suitable environment for rapid growth of subgrains during recovery [29,30]. Moreover, due to high local lattice rotations, growth of these nuclei's can also occur readily once the critical subgrain size is exceeded [29,30]. In general, recrystallisation nuclei are known to form at the matrix-shear band interfaces and also within the shear bands [29,30]. Nucleation at interfaces is known to promote rotated Cube orientation (rotated about ND), whereas nucleation within the shear bands leads to the development of Goss orientation [29,30]. Growth of rotated Cube and Goss orientation occurs readily due to favourable orientation relationship ($40^\circ < 111 \rangle$) with deformation texture components [29,30]. In the present scenario, texture intensity can be observed near rotated Brass position. Hence, it can be concluded that nucleation at shear bands is not operative in the present case.

In commercial Al alloys, nucleation can also occur near large particles owing to the presence of deformation zone near these particles [29,31,32]. The formation of deformation zone can be attributed to incompatibility issues at the matrix-particle interface [29,31,32]. As a result, large amount of geometrically necessary dislocations are stored near these particles which in turn result in development of lattice curvature [29,31,32]. It is well known that the orientations of subgrains within the deformation zones are fairly random and consequently, a very weak texture develops upon recrystallisation characterised by the presence of $\{011\}\{\bar{1}\bar{2}\bar{2}\}$ P orientation and rotation of Cube orientation about the normal direction [29,31,32]. In the present case, both these orientations were not observed upon annealing of cross rolled samples. Hence, nucleation near large particles can be ruled out.

Apart from the above-mentioned sites, grain boundaries between the deformed grains are also favourable sites for recrystallisation [33,34]. It is well established that significant amount of orientation gradient

is generally present in the regions close to grain boundaries owing to higher number of active slip systems in the grain boundary affected zone [33,34]. The higher number of active slip systems can be attributed to compatibility issues across the grain boundaries [33,34]. Hence, a suitable condition for recovery and subsequent formation of recrystallisation nuclei exists near grain boundaries [33,34]. The growth prospects of these nuclei's are also quite high due to existing high angle grain boundary between the deformed grains [33,34]. The nucleation at the grain boundary proceeds by strain-induced boundary migration (SIBM), namely growth of subgrains from one side of the grain boundary into the more heavily deformed grain on the other side of the boundary [33,34]. Hence, it can be contemplated that this mechanism will lead to formation of orientations similar to rolling texture components [29]. In the present case, it was observed that there was no characteristic difference between rolling texture and annealing texture. Hence, it can be concluded that nucleation at grain boundaries and SIBM mechanism is operative in the present case.

Conclusions

In the present work, the possibilities of improving formability of Al alloys via effective texture control were discussed. It was found that cross rolling can lead to the development of unique rotated Brass texture where cross-slip is hindered along all the three principal directions. This in turn can delay the onset of local necking and improve the formability of Al sheets. The other key findings are summarised below:

- (1) The sensitivity of necking strain (ε_N) towards cross-slip propensity (K_2) was highlighted based on the combination of Voce hardening equation and Considere's criteria.
- (2) The importance of texture control in terms of inhibiting cross-slip was highlighted via Schmid factor calculation for cross-slip system and the ratio of Schmid factor for leading and trailing partial.
- (3) The evolution of rotated Brass texture in the cross rolled sample was due to the back and forth movement of orientations between Brass and rotated Brass position owing to the constant change in rolling direction by 90° for each pass.
- (4) The evolution of recrystallisation texture for the cross rolled sample was due to strain-induced boundary migration mechanism as the same rotated Brass texture is also observed upon annealing. The other recrystallisation mechanisms such as due to cube bands, shear bands and particle stimulated nucleation cannot explain the recrystallisation texture of the cross rolled sample.

Acknowledgements

The authors would like to thank the Texture Lab, IIT Kanpur.

Disclosure statement

No potential conflict of interest was reported by the author(s).

ORCID

Mirtunjay Kumar  <http://orcid.org/0000-0002-5706-2283>

References

- [1] Ramezani M, Ripin ZM. Introduction to sheet metal forming processes. In: Ramezani M, Ripin ZM, editors. Rubber-pad forming processes. Cambridge, UK: Woodhead Publishing; 2012. p. 1–22.
- [2] Smith CB, Mishra RS. Fundamentals of formability. In: Smith CB, Mishra RS, editors. Friction stir processing for enhanced low temperature formability. Boston (MA): Butterworth-Heinemann; 2014; p. 7–9.
- [3] Sousa R. Incremental sheet forming technologies. Reference module in materials science and materials engineering. Amsterdam, Netherlands: Elsevier; 2016.
- [4] Marciniak Z, Duncan JL, Hu SJ. Load instability and tearing. In: Marciniak Z, Duncan JL, Hu SJ, editors. Mechanics of sheet metal forming. 2nd ed. Oxford: Butterworth-Heinemann; 2002; p. 61–81.
- [5] Ghosh AK. The influence of strain hardening and strain-rate sensitivity on sheet metal forming. J Eng Mater Technol. 1977;99(3):264–274. doi:10.1115/1.3443530.
- [6] Graf A, Hosford WF. Calculations of forming limit diagrams. Metall Trans A. 1990;21(1):87–94. doi:10.1007/BF02656427.
- [7] Mecking H, Kocks U. Kinetics of flow and strain-hardening. Acta Metall. 1981;29(11):1865–1875.
- [8] Kocks U, Mecking H. Physics and phenomenology of strain hardening: the FCC case. Prog Mater Sci. 2003;48(3):171–273.
- [9] Krausz AS, Krausz K. Unified constitutive laws of plastic deformation. San Diego (California): Elsevier; 1996.
- [10] Yasnikov I, Estrin Y, Vinogradov A. What governs ductility of ultrafine-grained metals? A microstructure based approach to necking instability. Acta Mater. 2017;141:18–28.
- [11] Vinogradov A, Yasnikov IS, Matsuyama H, et al. Controlling strength and ductility: dislocation-based model of necking instability and its verification for ultrafine grain 316L steel. Acta Mater. 2016;106:295–303.
- [12] Hosford WF, Fleischer RL, Backofen WA. Tensile deformation of aluminium single crystals at low temperatures. Acta Metall. 1960;8(3):187–199.
- [13] Mishra S, Yadava M, Kulkarni K, et al. A modified Taylor model for predicting yield strength anisotropy in age hardenable aluminium alloys. Mater Sci Eng: A. 2017;699:217–228.
- [14] Hosford WF. The mechanics of crystals and textured polycrystals. New York: Oxford University Press; 1993:248.
- [15] Cheng L, Poole W, Embury J, et al. The influence of precipitation on the work-hardening behaviour of the aluminium alloys AA6111 and AA7030. Metall Mater Trans A. 2003;34(11):2473–2481.
- [16] Poole* W, Wang X, Lloyd D, et al. The shearable–non-shearable transition in Al–Mg–Si–Cu precipitation

- hardening alloys: implications on the distribution of slip, work hardening and fracture. *Philos Mag.* **2005**;85(26-27):3113–3135.
- [17] Mori T, Fujita H. Effect of dislocation structure on the flow stress in Cu-3 at.% Al single crystals. *Philos Mag A.* **1982**;46(1):91–104. doi:10.1080/01418618208236210.
- [18] Kubin LP, Devincere B, Hoc T. Inhibited dynamic recovery and screw dislocation annihilation in multiple slip of fcc single crystals. *Philos Mag.* **2006**;86(25-26):4023–4036. doi:10.1080/14786430500525241.
- [19] Kubin L, Devincere B, Hoc T. Toward a physical model for strain hardening in fcc crystals. *Mater Sci Eng: A.* **2008**;483-484:19–24.
- [20] Samajdar I, Verlinden B, Van Houtte P, et al. γ -Fibre recrystallization texture in IF-steel: an investigation on the recrystallization mechanisms. *Mater Sci Eng: A.* **1997**;238(2):343–350.
- [21] Engler O, Hirsch J. Texture control by thermomechanical processing of AA6xxx Al–Mg–Si sheet alloys for automotive applications—a review. *Mater Sci Eng: A.* **2002**;336(1):249–262.
- [22] Stout MG, Chen SR, Kocks UF. Mechanisms responsible for texture development in a 5182 aluminium alloy deformed at elevated temperature. United States 1998; 11-15 Oct 1998; Rosemont, IL (United States): 1998 Minerals, Metals and Materials Society (TMS) fall meeting; **1998**.
- [23] Suwas S, Gurao N. Development of microstructures and textures by cross rolling. *Compr Mater Process.* **2014**;3:81–106.
- [24] Gurao NP, Sethuraman S, Suwas S. Effect of strain path change on the evolution of texture and microstructure during rolling of copper and nickel. *Mater Sci Eng: A.* **2011**;528(25):7739–7750.
- [25] Ray R. Rolling textures of pure nickel, nickel-iron and nickel-cobalt alloys. *Acta Metall Mater.* **1995**;43(10):3861–3872.
- [26] Leffers T, Ray RK. The brass-type texture and its deviation from the copper-type texture. *Prog Mater Sci.* **2009**;54(3):351–396.
- [27] Liu WC, Man CS, Morris JG. Lattice rotation of the cube orientation to the β fibre during cold rolling of AA 5052 aluminium alloy. *Scr Mater.* **2001**;45(7):807–814.
- [28] Hong S-H, Lee DN. Deformation and recrystallization textures in cross-rolled copper sheet. *J Eng Mater Technol.* **2002**;124(1):13–22.
- [29] Engler O. Nucleation and growth during recrystallisation of aluminium alloys investigated by local texture analysis. *Mater Sci Technol.* **1996**;12(10):859–872.
- [30] Engler O, Escher C, Gottstein G. Investigation of the Nucleation of Recrystallization in an Al–Cu single crystal by means of EBSP. *Materials Science Forum*; 1993: Trans Tech Publ.
- [31] Humphreys F. The nucleation of recrystallization at second phase particles in deformed aluminium. *Acta Metall.* **1977**;25(11):1323–1344.
- [32] Rollett A, Humphreys F, Rohrer GS, et al. Recrystallization and related annealing phenomena. Oxford: Elsevier; **2004**.
- [33] Bellier S, Doherty R. The structure of deformed aluminium and its recrystallization—investigations with transmission Kossel diffraction. *Acta Metall.* **1977**;25(5):521–538.
- [34] Dadson ABC, Doherty RD. Transmission pseudo-Kossel (TK) studies of recrystallized hot-deformed (dynamically recovered) polycrystalline aluminium. *Acta Metall Mater.* **1992**;40(8):2053–2058.